Direct Molecular Simulation of Nonequilibrium Dilute Gases

Thomas E. Schwartzentruber,* Maninder S. Grover,† and Paolo Valentini‡
University of Minnesota, Minneapolis, Minnesota 55455

DOI: 10.2514/1.T5188

This paper summarizes research performed over the past decade on the direct molecular simulation of dilute gas flows. Similar to the molecular dynamics method, a potential energy surface is the sole model input to a direct molecular simulation calculation. However, instead of simulating the motion of all atoms in the system deterministically, the direct molecular simulation method uses stochastic techniques and assumptions, adopted from the well-established direct simulation Monte Carlo method, which are accurate for dilute gases. Using the same potential energy surface as input, the direct molecular simulation method is verified to exactly reproduce pure molecular dynamics results for shock-wave flows. The direct molecular simulation method is then used to investigate nonequilibrium flows such as strong shock waves and dissociating nitrogen systems involving rotation–vibration coupling and coupling between internal energy and dissociation. Direct molecular simulation algorithms are detailed, and a number of new results relevant to hypersonic flows are presented along with a summary of other recent results in the literature.

I. Introduction

THE relevant governing equation for nonequilibrium dilute gases, when the molecular nature of the gas must be explicitly accounted for, is the Boltzmann equation. The Boltzmann equation determines the evolution of the velocity and energy distribution functions of atoms and molecules, locally at any point in the flow. In the near-equilibrium limit where velocity and energy distributions are Maxwell–Boltzmann or Chapman–Enskog, the Boltzmann equation reduces to the continuum Euler or Navier–Stokes equations, respectively. The Boltzmann equation is therefore useful as an accurate model for highly nonequilibrium flow conditions and is also useful to study near-equilibrium flows where molecular physics may have important macroscopic effect, such as the coupling between vibrational energy and dissociation.

When all relevant physics are included, the Boltzmann equation becomes highly multidimensional for chemically reacting gas mixtures, and partial differential equation based numerical solutions become intractable. Instead, the direct simulation Monte Carlo (DSMC) particle-based numerical method [1,2] has proven to be an accurate and efficient technique to simulate the physics contained in the Boltzmann equation. DSMC particles can have a species type, continuous or quantized internal energies (rotation and vibration), and collision probabilities, and the outcomes of each collision (including chemical reactions) can be determined solely from the properties of atoms and molecules. In the most general implementation, the probabilities of particles transitioning from any initial energy state to any final state, during a collision, can be specified as input to a DSMC simulation (these probabilities are called state-to-state cross sections). Currently, complete cross-section data cannot be measured experimentally. As a result, simplified cross-section models are used within DSMC, which are typically formulated to be consistent with empirical models already used in continuum Navier–Stokes calculations. This is not satisfactory for the study of highly nonequilibrium conditions, nor is it satisfactory when using molecular-level physics to develop new, or improved, continuum models for near-equilibrium flows.

More recently, computational chemistry is being used to determine cross sections for DSMC simulations. Theory from quantum mechanics is used to calculate the interactions between atoms, and using large parallel computer clusters, huge numbers of individual collisions are performed. The most common approach is called quasi-classical trajectory (QCT) analysis, and in principle, QCT analysis can determine all energy transition cross sections for use within DSMC. The result would be a predictive simulation capability (i.e., no empiricism) for nonequilibrium reacting flows over complex geometries. However, the problem is the vast number of possible energy transitions. For N_2–N_2 collisions, each of the N_2 molecules can transition from one of approximately 10,000 quantized rovibrational states to any other state. Therefore, the total number of transition cross sections for such collisions is on the order of $(10{,}000)^4/2 \approx 10^{15}$. This approach is intractable, even for zero-dimensional calculations. For atom–diatom collisions, involving fewer transition probabilities, this approach is barely tractable. For example, the N–N_2 collision system was analyzed by Kim and Boyd [3] and Panesi et al. [4]. Both studies used the same database of cross sections determined via QCT analysis using an ab intio potential energy surface (PES) [5]. The database exhibited large statistical scatter in individual cross sections (for example, refer to Fig. 3 in [6]), and as reported in [7], over 60% of the transition rates in the dataset had no value. More recently Andrienko and Boyd have performed master equation analysis for the O + O_2 collision system [8–10] and the N + O_2 collision system [11].

The large number of required cross sections necessitates further assumptions and simplifications. For example, compared to the ab initio PESs with large numbers of fitting coefficients, such as the N–N_2 PES discussed previously, PESs with simpler functional forms can be used to obtain more QCT results with less computational resources. Furthermore, many nearby energy states can be binned into a single energy group so that only a limited number of cross sections for transitions between energy groups are required [12]. In some cases, only individual vibrational energy states are considered, and probabilities are averaged over all rotational states. Aside from the energy transitions caused by collisions, the collision rate itself (the total cross section) may be dependent on the internal energy states of molecules, especially at high temperatures, where molecular bonds may be stretched due to rovibrational motion (see Fig. 11 in [13]), an effect that is commonly neglected. Finally, even for full state-to-state analysis involving all energy state transitions, the decoupling of internal energy into rotational and vibrational modes is not rigorous, especially at high temperatures. Both master equation analysis and state-to-state DSMC analysis suffer the same challenges. Of course, it is important to note that such simplifying assumptions may, in fact, be quite accurate. However, without a

Received 10 February 2017; revision received 0 ; accepted for publication 6 August 2017; published online 20 October 2017.

*College of Science and Engineering, Department of Aerospace Engineering and Mechanics; schwart@umn.edu.
†College of Science and Engineering, Department of Aerospace Engineering and Mechanics; grove311@umn.edu.
‡College of Science and Engineering, Department of Aerospace Engineering and Mechanics; vale0142@umn.edu.

baseline solution to the full problem, it is difficult to quantify the accuracy of such assumptions.

There is another approach that requires none of these simplifications and is computationally tractable for atom–diatom and diatom–diatom systems, even using ab initio PESs. The approach was first proposed by Koura [14,15], referred to as classical trajectory calculation (CTC)–DSMC. The basic premise is to perform trajectory calculations (on a PES) for each collision within a DSMC calculation. Essentially, instead of precomputing the probabilities of all possible energy transitions through large numbers of QCT calculations, the direct molecular simulation (DMS) method performs collision trajectories "on the fly" within a simulation of an evolving gas system. In this manner, the molecular state resulting from one collision becomes the initial state for the next collision. Instead of resolving all possible energy transitions, the DMS method automatically simulates only the most dominant energy transitions that actually occur with nonnegligible frequency for the conditions of interest. Although computationally demanding, this approach is now tractable for diatom–diatom systems and, in fact, for gas mixtures with a number of species combinations within collisions.

This paper summarizes recent research that has built upon the approach of Koura. The method has been incorporated into modern DSMC algorithms, extended to rotating and vibrating molecules, including dissociation reactions while employing ab initio PESs, and is now referred to as direct molecular simulation (DMS). This paper also presents new results using the DMS method for high-temperature flows involving rotation–vibration coupling and coupling between internal energy and dissociation.

II. Direct Molecular Simulation

A. Numerical Method

The direct molecular simulation method (DMS) simply embeds trajectory calculations within a standard DSMC simulation. The DSMC method [1,2] exploits three fundamental characteristics of dilute gases.

1) Molecules move without interaction for time scales given by the local mean collision time.

2) Impact parameters and initial orientations of colliding molecules are random.

3) There are an enormous number of molecules per cubic mean free path, and only a statistical representation of these molecules is required.

These are accurate and rigorous simplifications for dilute gases. However, the DSMC method then goes further and employs stochastic models to determine the collision rate and the outcome of collisions, thereby introducing empiricism and physical model uncertainty. The DMS method replaces these stochastic collision models with trajectory calculations performed on a PES. As a result, the only model input to a DMS calculation is the PES (or set of PESs), and as discussed in this paper, DMS effectively becomes an acceleration technique for molecular dynamics (MD) simulation of dilute gases.

The DMS method, also referred to as classical trajectory calculation DSMC (CTC–DSMC), was first proposed by Koura [14,15]. Here, we present an implementation using the no-time-counter (NTC) collision rate algorithm of Bird [1], which is more commonly used in modern DSMC codes [2].

During each DMS time step Δt_{DMS}, after particles are moved and sorted locally into collision cells, a fraction of the particles (both atoms and molecules) in each cell are selected to undergo trajectories. The standard NTC algorithm is used, where a maximum cross section $(\overline{\sigma g})_{\max}$ is first used as a conservative estimate for the number of trajectories to be performed:

$$N_{t,\max} = \frac{1}{2} N_p (N_p - 1) \frac{(\overline{\sigma g})_{\max} W_p \Delta t_{\mathrm{DMS}}}{V} \tag{1}$$

where N_p is the current number of particles in the cell, W_p is the particle weight (the number of real particles represented by each simulation particle), and V is the cell volume. Because of the discrete nature of the simulation this value must be rounded to the nearest integer,

$$N^*_{t,\max} = \mathbf{int}(N_{t,\max} + 0.5) \tag{2}$$

and because a particle should not undergo more than one collision per time step, this value should be further limited between

$$1 \le N^*_{t,\max} \le \mathbf{int}(N_p/2) \tag{3}$$

During each time step and within each cell, the NTC procedure consists of forming $N^*_{t,\max}$ particle pairs (randomly from the N_p particles within the cell) and accepting/rejecting each pair for a trajectory with the following probability P_t:

$$P_t = \frac{\sigma g}{(\overline{\sigma g})_{\max}} \left(\frac{N_{t,\max}}{N^*_{t,\max}} \right) \tag{4}$$

Here, g is the relative speed between the particle pair, and σ is the appropriate cross section for the pair. Within a DSMC calculation, a cross-section model is used for σ to achieve a physically accurate collision rate (and accurate gas transport properties in the limit of near-equilibrium). However, within a DMS calculation, a conservative hard-sphere cross section is used:

$$\sigma = \pi b^2_{\max} \tag{5}$$

where it is crucial that the value of $b_{\max}$ is the maximum impact parameter used for each trajectory calculation, as described in the next section. The value of $(\overline{\sigma g})_{\max}$ can be set as a conservatively large constant, or its value is often updated and stored within each cell based on the maximum value experienced previously in the cell, so that the value of P_t remains less than unity. Note that, because P_t is applied to each of the $N^*_{t,\max}$ pairs, the total number of trajectories selected for the cell, proportional to $N^*_{t,\max} \times \langle P_t \rangle$, is not dependent on the value of $(\overline{\sigma g})_{\max}$; rather, its value is only set to improve computational efficiency.

Therefore, within each cell and during each time step, pairs of particles are selected for trajectory calculations using Eqs. (1–5). As described by Boyd and Schwartzentruber [2] the NTC method can be used, unaltered, for gas mixtures and will automatically select appropriate species-pairings for trajectories.

For zero-dimensional DMS calculations, only one cell is required, particle movement and position is irrelevant, and therefore Eqs. (1–5) are the only additional equations required beyond a standard trajectory code (i.e., a QCT code). Furthermore, for steady-state DMS flows (Secs. III.B and III.C), relatively few particles are required per cell ($N_p \ge 20$), and quantities can be sampled over many time steps during steady state, whereas for unsteady flows (Sec. IV), N_p may need to be very large (possibly millions of particles) to resolve evolving distribution functions where state populations can span many orders of magnitude.

B. Trajectory Calculations and Parallel Implementation

1. *Trajectory Integration*

As depicted in Fig. 1, for each particle pair accepted for a trajectory using Eq. (4), a standard trajectory calculation is performed using a PES. In fact, a library of PES subroutines may be available, and depending on the species pair selected, the appropriate PES subroutine can be used to integrate the trajectory, thereby enabling DMS calculations of gas mixtures. We use the algorithms from the REAQCT code described in [16]; however, any trajectory code and PES can be used as a "black-box" subroutine.

Ultimately, the trajectory code requires the initial positions and velocities of all atoms for each of the two particles. For molecules, positions and velocities relative to the center of mass are required to specify the rotational and vibrational state, which could correspond to a quantum state (v, j) or a classical energy state (ϵ_{vib}, ϵ_{rot}). A relative velocity of g is given to the particles (and atoms that comprise them), and the particles are separated at some conservative

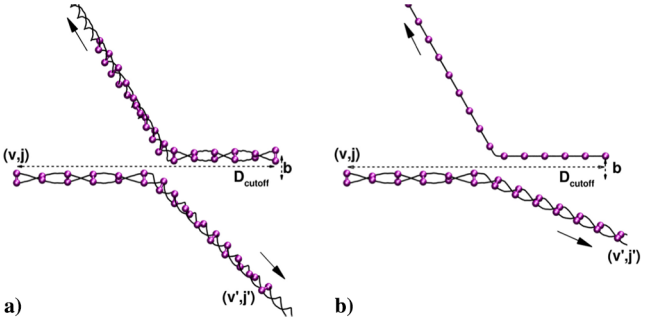

Fig. 1 Example of N_2–N_2 and N–N_2 trajectories.

distance D_{cutoff}, and positioned with an impact parameter b that is properly randomized within the range

$$0 \leq b^2 \leq b_{\max}^2 \tag{6}$$

where $b_{\max}$ must be the same value used in Eq. (5). The PES is then used to integrate the equations of motion for the atoms in the system.

2. *Pre- and Postcollision States*

Simple rules can be implemented to determine when particles are no longer interacting and therefore when to stop the trajectory calculation as well as to determine which atoms are bound within any product molecules. Therefore, any type of trajectory outcome, allowed by the PES, can be simulated and analyzed within a DMS calculation, including exchange, dissociation, swap dissociation, and double-dissociation reactions [16].

Within a DMS calculation, the posttrajectory properties must be associated with (stored in memory for) each DMS particle because, unlike QCT, DMS particles move through the domain and are selected for additional trajectory calculations in subsequent time steps. In general, given the posttrajectory atom positions and velocities, new DMS particle velocity vectors (center-of-mass velocities) can be determined, and internal energy states (for molecules) can be determined using one of three strategies.

1) Determine and store the corresponding quantized state (v, j) using a classical-quantum binning procedure.

2) Determine and store the corresponding classical energies and instantaneous bond distance (ϵ_{vib}, ϵ_{rot}, and d_{bond}).

3) Simply store the positions and velocities of all atoms (i) comprising the particle ($\bar{x}_i$, $\bar{v}_i$).

Strategy 1 has not yet been tested in DMS. Strategy 2 works well for bound molecules and is used in Sec. III.B. Whereas the angular momentum of a rotating, vibrating molecule is conserved during free flight, classically defined values of ϵ_{rot} and ϵ_{vib} oscillate depending on the instantaneous value of d_{bond} (discussed at length in Sec. 5.6.1 of [17]). Therefore, in addition to storing ϵ_{rot} and ϵ_{vib} (standard DSMC variables), storing the additional variable d_{bond} enables the precise molecular state to be regenerated before the particle's next trajectory. It is important to note that strategy 2 does not make any assumptions about decoupling rotational and vibrational energy within the DMS simulation; the variables ϵ_{rot}, ϵ_{vib}, and d_{bond} are only used to regenerate/record the atom positions within a molecule before/after each trajectory. For simulations involving chemical reactions (Sec. IV), where molecular bonds can be highly stretched, strategy 2 has not proven successful, and we use strategy 3. Strategy 3 requires the storage of more quantities for each DMS simulation particle; however, it has proven to be accurate and robust for a number of PESs and gas conditions.

3. *Maximum Impact Parameter*

When describing the DMS method and, in particular, the value of $b_{\max}$ [Eqs. (5) and (6)], it is useful to distinguish a difference between trajectories and "collisions". Specifically, we refer to a collision as a trajectory that results in a finite deflection angle or some finite change in particle properties. If a large value is chosen for $b_{\max}$, then the number of particle pairs accepted for trajectories will be large because Eq. (4) is proportional to σ. However, many of these trajectories will be initialized with large impact parameters [Eq. (6)], and therefore, in many of these trajectories, the two particles will not "collide" (no change in particle velocities or internal energies). As the value of $b_{\max}$ is lowered, fewer trajectories are simulated; however, because these trajectories are initialized with smaller b values, a larger fraction will result in a collision. In fact, it is the PES that determines the collision rate, regardless of the number of particles pairs accepted for trajectories. Of course, if $b_{\max}$ is too small, then all trajectories will result in a collision, and the collision rate is no longer determined by the PES; rather, it is now restricted to the hard-sphere collision rate corresponding to the small value of $b_{\max}$, resulting in an inaccurate collision rate that is too low.

The effect of $b_{\max}$ is clearly shown in Fig. 2 for DMS simulations of a normal shock wave in nitrogen (full details of these simulations and the PES are provided later in Sec. III.B). The computed temperature profiles within the shock wave are shown for three different $b_{\max}$ values. As seen in Fig. 2a, the DMS solution does not change when $b_{\max}$ is lowered from 15 to 4 Å. This result is consistent with the QCT analysis of Bender et al. [16], which showed no interaction for N_2–N_2 collisions for impact parameters of 6 Å and larger. When $b_{\max} = 15$ Å, the simulation is computationally inefficient because a large number of trajectories are simulated in each cell during each time step that result in no interaction at all. When $b_{\max} = 4$ Å, the same solution is obtained with far fewer simulated trajectories. As $b_{\max}$ is lowered below 4 Å, noticeable error is introduced. As seen in Fig. 2b, when $b_{\max} = 1.75$ Å, the solution is consistent with a low collision rate (causing increased molecular transport throughout the shock wave), resulting in a thick shock wave that does not even reach thermal equilibrium in the postshock region.

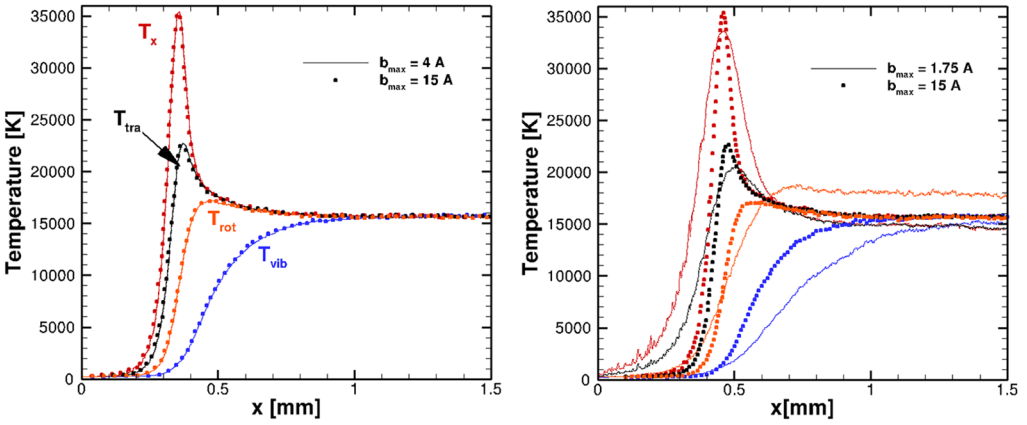

a) Conservatively large value of b_{max} **b) Small value of b_{max}**

Fig. 2 Effect of varying $b_{\max}$ on shock profiles.

Clearly, as long as a conservative value of b_{max} is chosen, it is the PES alone that determines the collision rate, regardless of the number of trajectories calculated per time step. This is perhaps the most crucial aspect of the DMS method. The result is that the only model input to a DMS calculation is the PES (similar to molecular dynamics), which determines both the local collision rate and collision outcomes including all relevant atomic-level physics with no decoupling of rotational and vibrational states. As described in the next section, DMS effectively becomes an acceleration technique for MD simulation of dilute gases.

4. *Parallel Implementation Strategies*

Two parallel implementations of the DMS method are used in this paper. The first implementation combines trajectory algorithms within the Molecular Gas Dynamic Simulator (MGDS) code (a parallel DSMC code developed at the University of Minnesota [18,19]). Here, the stochastic DSMC collision algorithms are simply replaced by the trajectory algorithms outlined previously, and extra variables are created to store the new particle information required by technique 2 or 3 discussed previously. All other aspects of the MGDS code, including the parallelization strategies, are unaltered, and two-dimensional (2-D) and three-dimensional (3-D) DMS simulations over complex geometry can be performed.

The second implementation is designed specifically for time-accurate, zero-dimensional (0-D), DMS calculations only. In this case, particle position and movement are not relevant, and a single partition stores the details of all simulation particles and selects particle pairs for trajectories using Eqs. (1–5). The particle pairs selected at each time step are then communicated to, and distributed among, a large number of partitions/processors for efficient parallel computation of the trajectories. The postcollision states are then communicated back to the main partition in preparation for the next time-step iteration. In fact, this DMS implementation and the REAQCT code [16], used for large batches of QCT calculations, use the same source code for parallelization. The important point is that, given an existing QCT code, it is a trivial extension to perform 0-D DMS calculations, essentially requiring only the allocation of an array of particle structures and the addition of Eqs. (1–5).

C. Verification with Molecular Dynamics

A series of studies were performed by Valentini et al. where shock waves in argon [20,21], mixtures of argon, helium, and xenon [22], and shock waves and expansions in diatomic nitrogen [23] were studied using pure molecular dynamics (MD) in the dilute gas regime. Such MD calculations are deterministic where the position and momenta of all atoms in the flow volume are advanced by solving the equations of motion with femtosecond-scale time steps. Because the same PES can serve as the sole model input for both DMS and MD calculations, comparison between DMS and pure MD can directly verify the techniques/assumptions (see items 1–3 discussed in Sec. II.A) employed by the DMS method.

Norman et al. demonstrated that DMS (CTC–DSMC) exactly reproduces pure MD simulations, at the level of the velocity and rotational energy distribution functions, for normal shock waves in argon and diatomic nitrogen [24]. For example, a Mach 7 nitrogen shock wave with preshock conditions of $\rho_1 = 0.1$ kg/m^3 and $T_1 = 28.3$ K was simulated using DMS and pure MD. The site-to-site Lennard–Jones potential was used to determine forces between atoms of different nitrogen molecules, and for atoms of the same molecule, the bond length was held fixed using the RATTLE algorithm [25]. Therefore, only translational–rotation energy transfer was simulated in both DMS and MD. The temperature and density profiles within the shock wave are shown in Fig. 3a, where precise agreement is found for both parallel (T_x) and normal (T_{yz}) translational temperature components as well as the rotational temperature and density profiles. Figure 3b presents DMS and MD calculations of diatomic nitrogen where the Ling–Rigby potential is used to determine forces between atoms of different molecules, and a harmonic oscillator (HO) potential is used to determine forces between atoms of the same molecule. Because the HO potential ensures bound molecules, both DMS and MD model translational–rotational–vibrational energy transfer but no chemical reactions. The shock-wave conditions are $M_1 = 7$, $T_1 = 2500$ K, and $\rho_1 = 0.5$ kg/m^3. As is evident from Fig. 3b, the temperature profiles match up precisely, within statistical uncertainty, which is very low for these simulations. Note that the relatively high density and high freestream temperature result in fewer molecules per cubic mean free path and a shorter vibrational relaxation time and therefore shorter domain length. This is necessary for the pure MD simulations to remain computationally tractable. In Sec. III.B, DMS alone is used to simulate shock-wave conditions directly relevant to hypersonic vehicles.

In Fig. 4, the rotational energy distribution functions corresponding to various positions within the shock wave from Fig. 3a, computed using pure MD, are compared against DSMC results (Fig. 4a) and against DMS results (Fig. 4b). The distributions exhibit non-Boltzmann behavior within the shock and reach a Boltzmann distribution as the gas nears the postshock region. The most important aspect of Fig. 4 is that the DSMC results used a new translational–rotational collision model, called the nonequilibrium direction-dependent model, that was developed specifically to reproduce the MD simulation results [26]. Noticeable discrepancy between DSMC and MD is observed, even using a DSMC model tailored to the MD result (Fig. 4a), whereas the agreement between DMS and MD is exact (Fig. 4b). This fact supports the conclusion that DMS acts as an acceleration technique for the MD simulation of dilute gases.

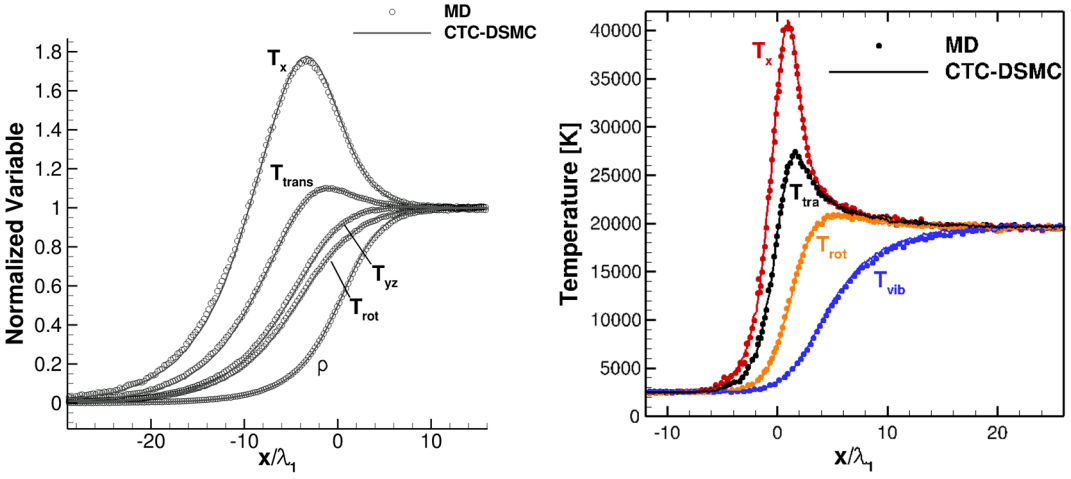

a) Rotational energy excitation b) Rovibrational energy excitation

Fig. 3 Comparison between shock profiles predicted by DMS and MD.

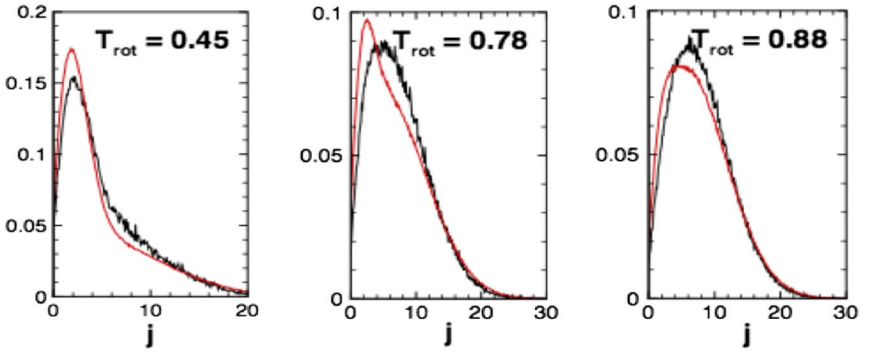

a) MD results (black lines) compared to DSMC results (red lines)

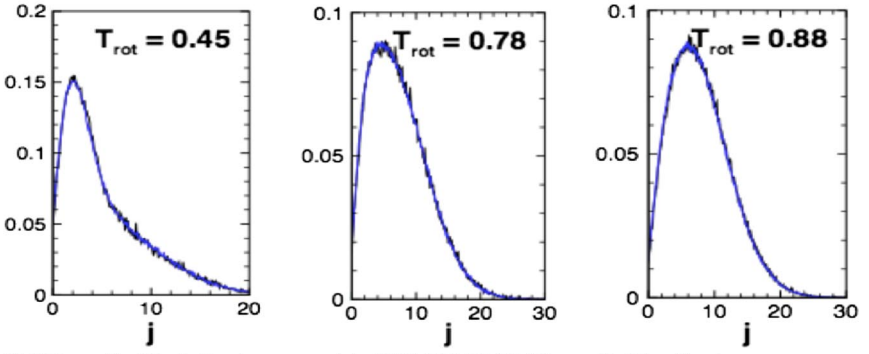

b) MD results (black lines) compared to CTC-DSMC (DMS) results (blue lines)

Fig. 4 Rotational energy distribution functions within the shock wave in Fig. 3a. Further details regarding these simulations can be found in [24,26].

Finally, DMS has also been shown to capture long-lived "orbiting" collisions. When the collision energy is sufficiently low, relative translation energy can be temporarily transferred to rotational energy, leaving insufficient translational energy for the pair to escape the weak attractive force between them. This results in long interaction times before the molecular orientations and translational energy are such that the pair separates. Such long-lived collisions are thought to be important for three-body collisions and therefore recombination reactions. In fact, preliminary algorithms to extend DMS to three-body collisions have been proposed [27], and it seems possible that DMS may be able to reproduce pure MD simulations that include three-body interactions and recombination reactions. The DMS method has many similarities with pure molecular dynamics and may have application outside of the high-temperature reacting flows discussed in this paper. For example, Bruno et al. [28] have recently used DMS (referred to as CT–DSMC) to study oxygen transport properties.

III. Rovibrational Coupling

As described previously in Sec. II.B.2, no decoupling of rotational and vibrational energy occurs during a DMS calculation. Rather, the method operates only on atom positions and velocities, and rotational/vibrational energies or quantized states are only obtained as a postprocessing step. Thus, the method accurately simulates rovibrational coupling according to the PES with no further assumptions.

A. Zero-Dimensional Relaxation

In a paper by Valentini et al. [29], rovibrational coupling was studied using DMS for zero-dimensional relaxation calculations in nitrogen. It was found that, under high-temperature conditions, the Jeans and Landau–Teller models could not reproduce the DMS results, which clearly showed additional rotation–vibration coupling. An example result is shown in Fig. 5a, where molecules are initiated in translational–rotational equilibrium, but with substantially lower vibrational energy. In this simulation, the center of mass translational energies of the N_2 molecules are resampled from a Maxwell–Boltzmann distribution at each time step, and the atom velocities are adjusted accordingly, to maintain isothermal conditions for the translational temperature. In this case, because the Jeans equation only models translation–rotation energy transfer (with a time constant τ_{rot}), the Jeans model would maintain translational–rotational equilibrium. Because the Landau–Teller equation only models translation–vibration energy transfer (with time constant τ_{vib}), the vibrational energy would not influence, nor be influenced by, the rotational energy at all. This is in contradiction to the DMS results, which show that energy is transferred from rotation into vibration.

The DMS simulation in Fig. 5a used the Ling–Rigby and HO potentials (as described for the result in Fig. 3b) and was performed for a very high temperature of 40,000 K. However, DMS simulations using the Taylor-6 oscillator (T-6) potential were also performed, and it was concluded that, as the degree of anharmonicity is increased, noticeable rovibrational coupling is observed at progressively lower temperatures [29]. The difference between HO, T-6, and a more realistic Morse potential is shown in Fig. 5b. Greater anharmonicity enables larger bond stretching for a specific vibrational energy and therefore greater coupling with the rotational energy. These zero-dimensional results, exhibiting rovibrational coupling, motivated the studies involving shock waves presented next.

B. Normal Shock Waves

Here, we present DMS simulation results for normal shock waves with freestream conditions relevant to hypersonic flight vehicles. Specifically, conditions were extracted from the 1976 Standard Atmosphere model at 40 km altitude ($\rho_1 = 0.0037$ kg/m^3 and $T_1 = 251.05$ K). Normal shock waves were generated for freestream velocities of $u = 3599.6$, 5154.4, 6459.6, and 8206.9 m/s, which produce postshock temperatures of approximately $T_2 = 5000$, 10,000, 15,000, and 25,000 K, respectively. These conditions are relevant to hypersonic aircraft and reentering spacecraft, as well as missile applications [30,31].

Similar to the results shown in Sec. III.A, the Ling–Rigby potential is used combined with either the HO or T-6 potential shown in Fig. 5b. Therefore, molecules remain bound at all times, and no chemical

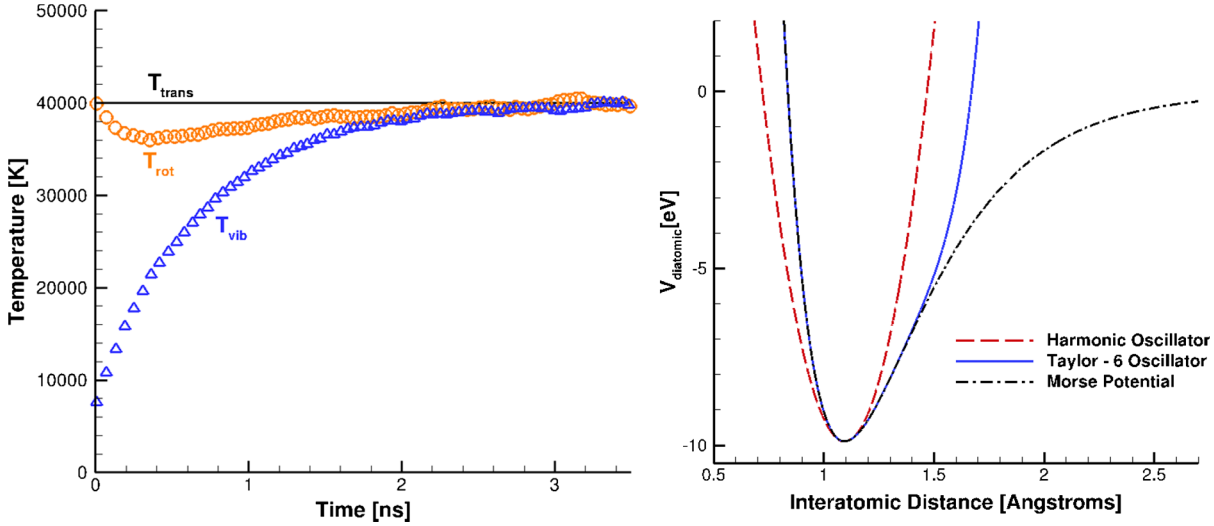

a) Rovibrational coupling in a heat bath

b) Intramolecular potentials with varying degrees of anharmonicity

Fig. 5 Rovibrational coupling effects.

reactions occur in the shock-wave simulations. Certainly, dissociation reactions would occur under the conditions studied, however, it is useful to prohibit chemical reactions to study rovibrational coupling. Finally, to manage pre- and posttrajectory molecular states and atom positions/velocities, the DMS simulations presented in this section employ strategy 2 discussed in Sec. II.B.2 and the parallel MGDS implementation discussed in Sec. II.B.4.

The temperature profiles resulting from each normal shock DMS calculation are shown in Fig. 6. For a postshock temperature of 5000 K (Fig. 6a), rotational energy excitation is orders of magnitude faster than vibrational excitation. Rotational energy quickly equilibrates with translational energy, and vibrational energy proceeds to excite slowly toward the transrotational energy. As shown in Fig. 6a, DMS simulations using both the HO and T-6 potentials produce nearly identical results, and no rovibrational coupling effects are observed. For postshock temperatures of 10,000 and 15,000 K (Figs. 6b and 6c), rovibrational coupling effects are now evident (only the T-6 results are plotted for clarity). The identifying feature is that the rotational temperature does not immediately reach the translational temperature; rather, the rotational temperature peaks and begins to decrease before equilibrating with translation. The Jeans equation, which only models translation–rotation energy transfer cannot capture this trend and, instead, would result in the rotational energy always increasing toward the translational energy. This trend is most clear for the DMS calculation with a postshock temperature of 25,000 K (Fig. 6d) where rotational and vibrational temperatures appear to equilibrate with each other prior to equilibrating with the translational temperature.

If a more realistic Morse potential (shown in Fig. 5b) is used, the degree of rovibrational coupling is expected to increase and be noticeable for lower postshock temperatures, although the overall temperature profiles are not expected to change significantly. Practically, it would be interesting to quantify how changes in rotational and vibrational energies due to coupling actually influence the rate of dissociation, in comparison to models that decouple rotational and vibrational energy transfer. This is difficult because, for high temperatures, where coupling is significant, dissociation is likely occurring during rovibrational excitation. To investigate all processes simultaneously, zero-dimensional DMS simulations of dissociating nitrogen, using both a Morse and ab initio-based PES, are presented in Sec. IV.

C. Multidimensional Flows

Because DMS has been implemented within the MGDS parallel DSMC code, two- and even three-dimensional DMS simulations are possible. An example DMS solution, using the Ling–Rigby + HO potentials, for Mach 20 nitrogen flow over a 6-cm-diam cylinder (with freestream values of $\rho = 0.8 \times 10^{-4}$ kg/m^3 and $T = 600$ K), is shown in Fig. 7a. Analogous to a DSMC simulation, a DMS solution is first obtained on a uniform grid, after which adaptive mesh refinement (AMR) is performed, and a new solution is obtained. The AMR process was repeated twice, resulting in the grid shown in Fig. 7a. Each cell is refined below the local mean free path scale, variable time steps are prescribed in cells (set below the local mean collision time scale), and each cell contains at least 10 molecules.

During the movement step, molecules' center-of-mass velocities are specularly reflected if they hit the symmetry boundary, and atom velocities are updated appropriately. Particles that hit a surface element are diffusely reflected with full thermal accommodation. Specifically, atom positions and velocities relative to the center of mass are reset to match rotational and vibrational energies sampled from Boltzmann distributions corresponding to the wall temperature (set to 1000 K). The simulations use strategy 3 to store atom positions and velocities that define the molecular state.

Temperature profiles along the stagnation line are plotted in Fig. 7b. The expected trend of coupled translational–rotational–vibrational excitation within a diffuse shock wave is observed, followed by the approach to thermal equilibrium in the high-density region next to the cylinder surface. Although a pure DSMC simulation of this flow requires approximately one CPU for a few hours, the DMS calculation requires approximately 312 core processors for 5 h. Clearly, 2-D/3-D DMS calculations are computationally expensive. However, this example simulation demonstrates that it is now possible to simulate macroscopic dilute gas flows over complex geometries where a PES acts as the sole model input.

IV. Chemically Reacting Systems

In this section, we present DMS results for dissociating nitrogen systems. We use the ab initio PES developed by Paukku et al. [32] in the Department of Chemistry at the University of Minnesota. After initial construction, the PES was modified slightly for use in a QCT study of nitrogen dissociation by Bender et al. [16]. The PES code is freely available online [33], and this exact source code is called as a subroutine within the DMS code to evaluate forces between atoms during DMS trajectories. The PES is accurate for both N_2–N_2 collisions and N–N_2 collisions [32], where, for N–N_2 collisions, the position of one N atom is held fixed at a far distance, while forces on the remaining three N atoms are evaluated [34]. The ab initio PES is far more computationally expensive to evaluate compared to simple potentials such as Ling–Rigby and Morse. As a result, we restrict our

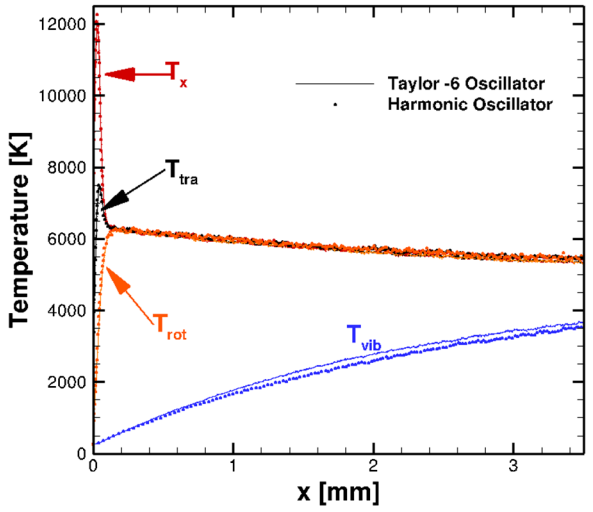

a) Post-shock temperature of 5000 K

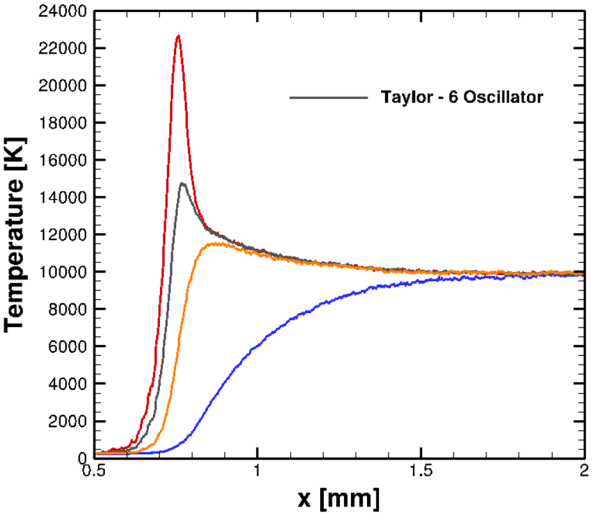

b) Post-shock temperature of 10,000 K

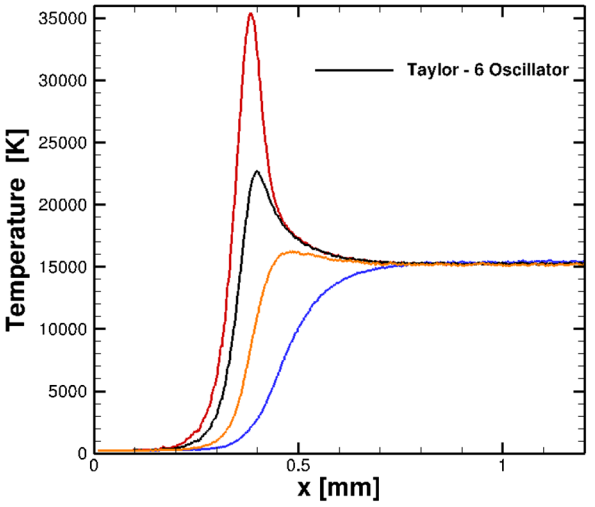

c) Post-shock temperature of 15,000 K

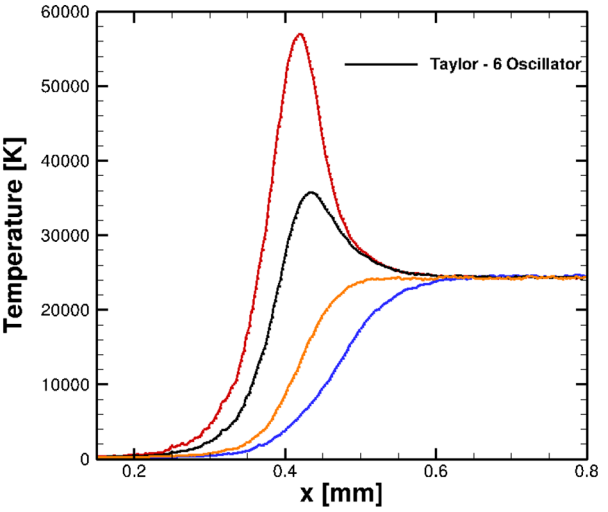

d) Post-shock temperature of 25,000 K

Fig. 6 Nonreacting DMS solutions for shock-wave profiles corresponding to hypersonic flight at approximately 40 km altitude.

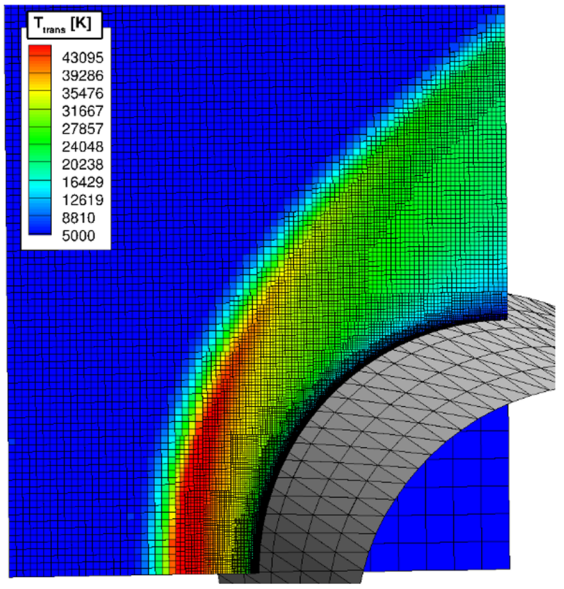

a) 2D temperature field and simulation grid

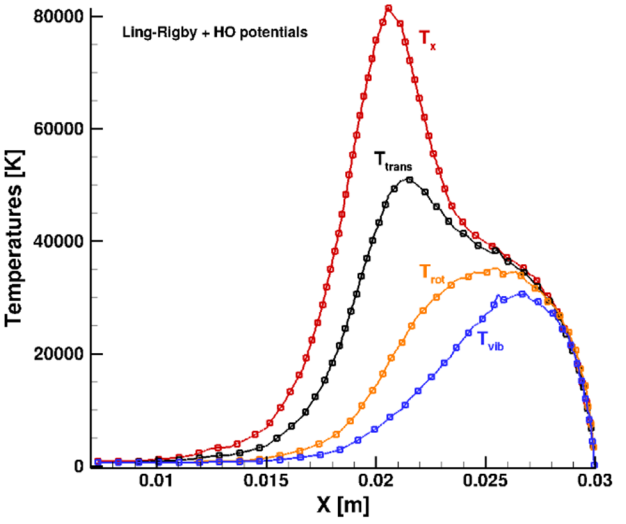

b) Stagnation line profiles

Fig. 7 Two-dimensional DMS simulation of hypersonic nitrogen flow over a cylinder.

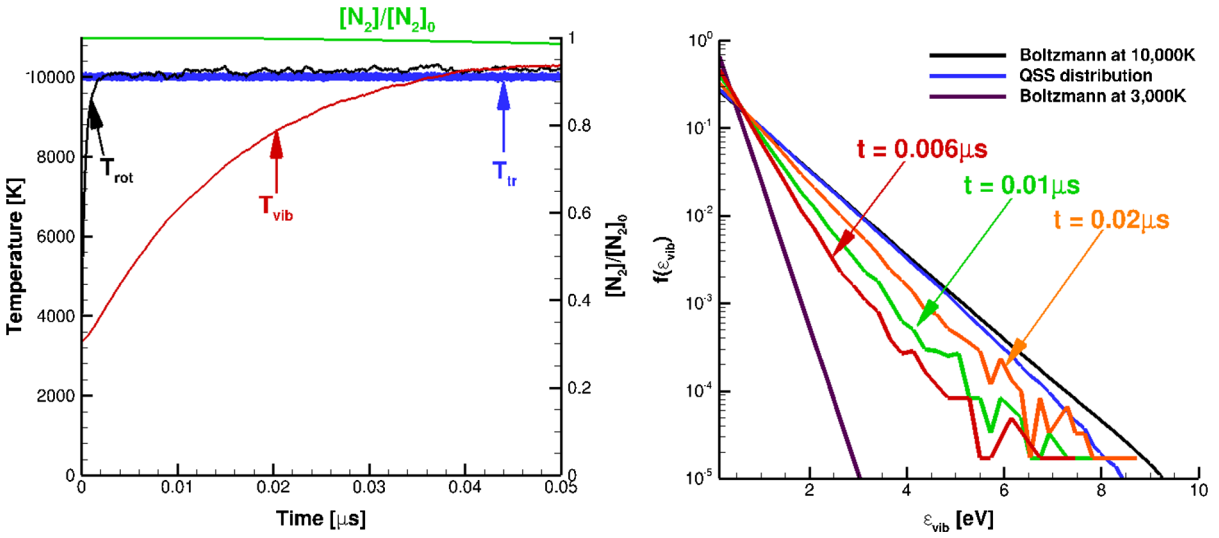

a) Temperature and species histories b) Transient vibrational distributions

Fig. 8 DMS results for nitrogen exciting to 10,000 K.

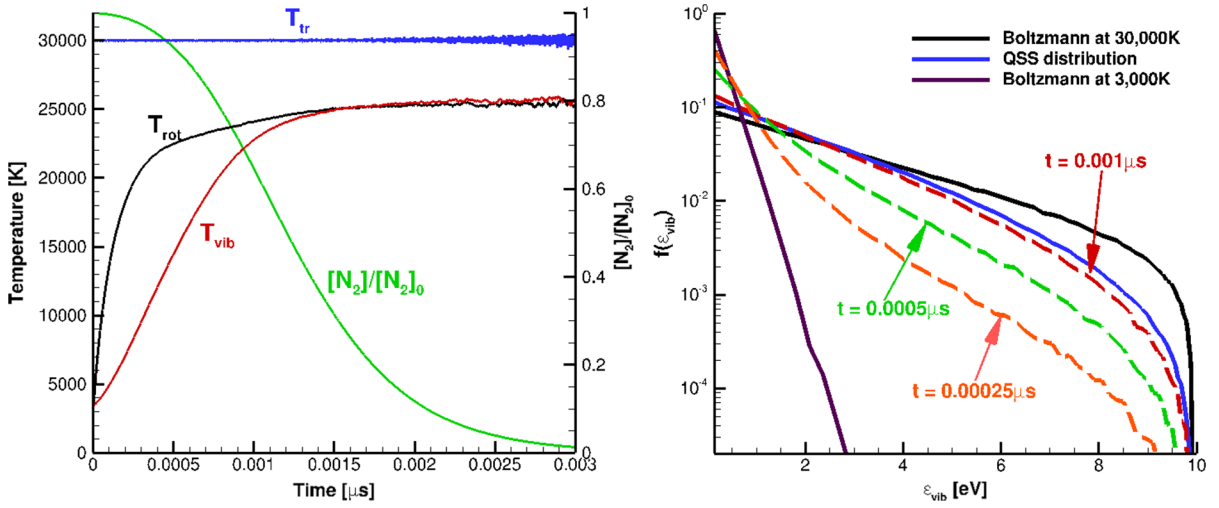

a) Temperature and species histories b) Transient vibrational distribtuions

Fig. 9 DMS results for nitrogen exciting to 30,000 K.

analysis to 0-D isothermal relaxation simulations and use the second DMS implementation discussed in Sec. II.B.4, which scales very well on large numbers of CPUs.

DMS predictions for a dissociating nitrogen system are shown in Figs. 8 and 9. The volume is initialized with N_2 molecules with rotational and vibrational energies sampled from a quantized Boltzmann distribution corresponding to the ab initio PES, following the procedure described by Bender et al. [16]. For postprocessing, atom positions and velocities are used to calculate the rovibrational energy of each molecule, and we use the vibrationally favored framework proposed by Jaffe [35] (also described in [16]) to separate this energy into ϵ_{rot} and ϵ_{vib}. We then define temperature in terms of the average energy in mode i, denoted as $\langle \epsilon_i \rangle$:

$$T_i \equiv \langle \epsilon_i \rangle / k_B \tag{7}$$

where $i =$ tra, rot, vib, and k_B is the Boltzmann constant.

For an isothermal DMS calculation where T_{tra} is maintained at 10,000 K and initially $T_{\text{rot}} = T_{\text{vib}} = 3000$ K, the molecules excite rotationally and vibrationally before any significant dissociation occurs. As seen in Fig. 8a, rotational energy excitation is much more rapid than vibrational energy excitation. In this case, although some number of N–N_2 collisions occur, the vast majority of collisions are N_2–N_2. The evolution of the vibrational energy distribution function (EDF) is shown in Fig. 8b. The vibrational EDFs appear to excite as a series of Boltzmann distributions, down to four orders of magnitude in population, approximately. Ultimately, the vibrational EDF reaches a QSS profile, exhibiting a depletion of high ϵ_{vib} levels compared to the Boltzmann result at 10,000 K. Even a slight depletion of high ϵ_{vib} levels has been shown to affect the computed dissociation rate [36].

As seen in Fig. 9a, for an isothermal DMS calculation where T_{tra} is maintained at 30,000 K and initially $T_{\text{rot}} = T_{\text{vib}} = 3000$ K, the molecules excite rotationally and vibrationally and begin to dissociate into N atoms. Both N_2–N_2 and N–N_2 trajectories are integrated using the ab initio PES, whereas for N–N collisions, postcollision velocities are simply sampled from a Maxwell–Boltzmann distribution corresponding to 30,000 K.

A first observation is that rotational energy excites faster than vibrational energy; however, their excitation rates are much closer compared to the 10,000 K case. This is due to the high translational energy but is also due to the fact that N atoms are very efficient at vibrationally exciting N_2 molecules through exchange reactions ($N_aN_b + N_c \rightarrow N_cN_b + N_a$) [34]. Because significant dissociation occurs during the rovibrational excitation, N atoms and associated exchange collisions result in an increased vibrational excitation rate. A second observation is that the rotational and vibrational energy of N_2 does not equilibrate with the translational energy; rather, a quasi-

steady state (QSS) is reached where internal energy is suppressed below the translational energy. This is due to internal energy excitation processes being balanced by the removal of internal energy due to dissociation reactions.

The evolution of the vibrational EDF, plotted at various times during the DMS simulation, is shown in Fig. 9b. For reference, equilibrium Boltzmann distributions corresponding to 3000 K and 30,000 K (based on the ab initio PES) are also plotted. At early times

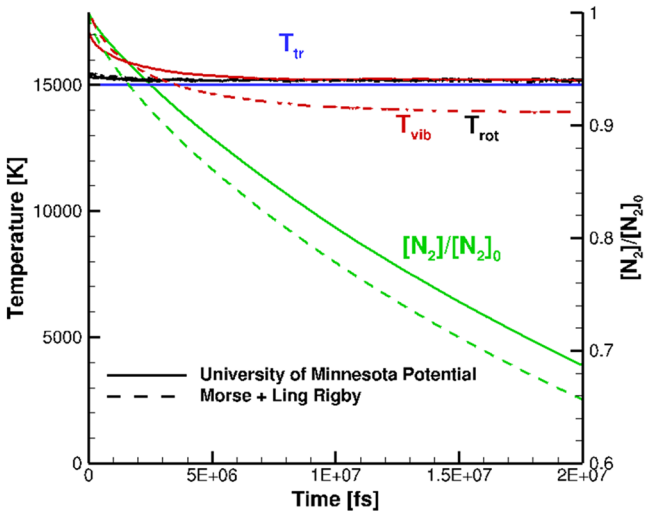

a) Macroscopic variables for 15,000 K

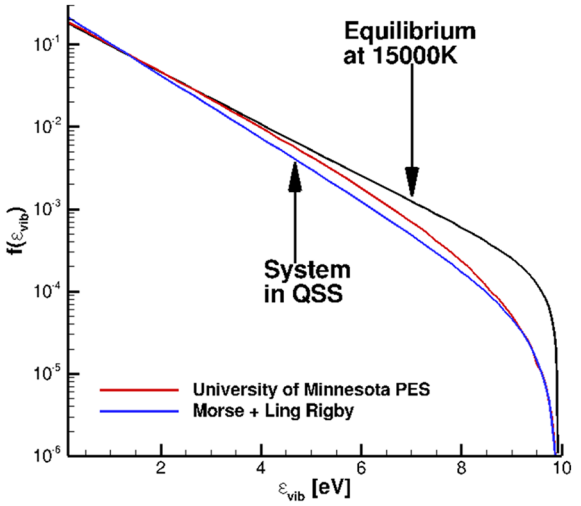

b) Molecular distributions for 15,000 K

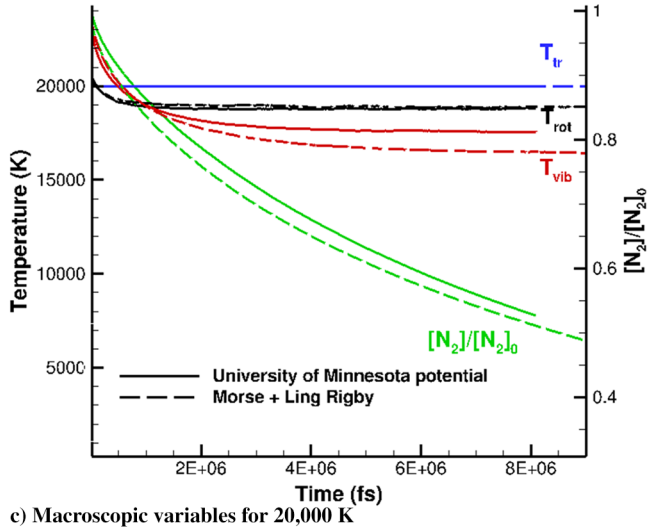

c) Macroscopic variables for 20,000 K

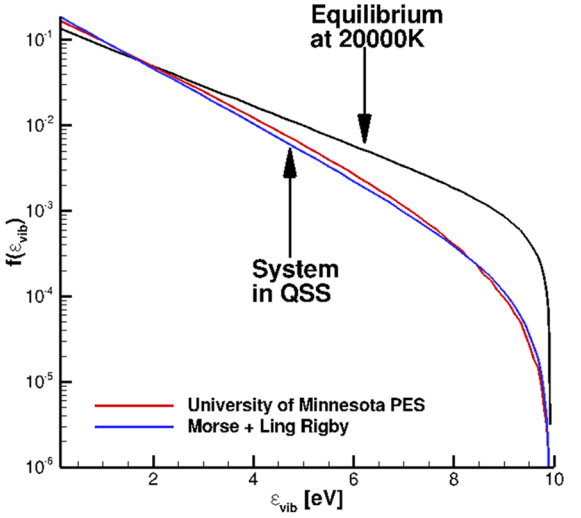

d) Molecular distributions for 20,000 K

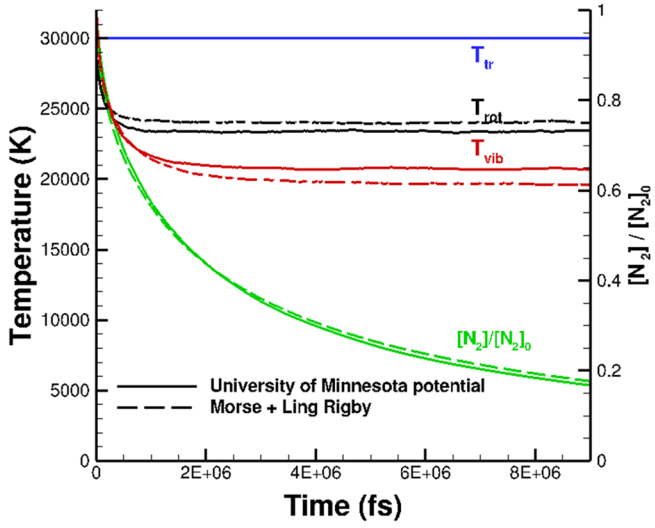

e) Macroscopic variables for 30,000 K

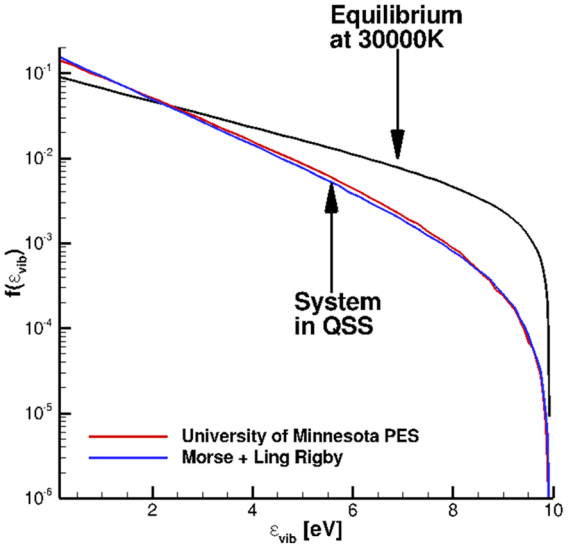

f) Molecular distributions for 30,000 K

Fig. 10 DMS isothermal relaxation results for the N_2–N_2 system using both ab initio and Ling–Rigby + Morse potentials.

τ_1 and τ_2, the vibrational EDF follows a Boltzmann distribution only for the lowest-energy states, whereas the high-energy tails are overpopulated. Then, within the QSS, the high-energy tail is depleted. Therefore, molecules' vibrational energy is rapidly excited to high levels; however, such high levels are strongly favored for dissociation reactions, and therefore the high-energy tail becomes depleted. Compared to dissociation rates calculated assuming Boltzmann EDFs, effective dissociation rates during this DMS calculation would be higher during the excitation phase (overpopulation) and lower during the QSS (depletion). These phenomena are described in detail and quantified in recent articles by Valentini et al. [34,36].

Similar to full master equation analysis, DMS captures the evolution of non-Boltzmann energy distributions as well as the coupling between translational–rotational–vibrational energy and dissociation. However, currently, master equation analysis for such a system is not possible due to the intractable number of energy state-transitions that must be precomputed. Full master equation results have only been presented for atom–diatom collisions, whereas the DMS results shown in Figs. 8 and 9 simulate the full nitrogen system including atom–diatom and diatom–diatom collisions as they occur concurrently within the evolving nitrogen system. Such DMS solutions can be used to verify the accuracy of nonequilibrium models and associated assumptions such as decoupling rotational and vibrational energy, grouping energy states into larger bins, averaging over the rotational energy mode, or models based only on average energy (i.e., multitemperature models). For example, Kulakhmetov et al. [37] recently proposed a maximum-entropy-based model for the $O + O_2$ collision system, and Singh et al. have proposed a new two-temperature model based on DMS and QCT results for the full nitrogen system [38].

An important advantage of the DMS method, compared to master equation and state-resolved approaches, is that one can quickly compare macroscopic results produced by different PESs without the need to construct multiple databases of transition rates (or cross sections).

In Fig. 10, the DMS method is used to compare rovibrational relaxation and dissociation predicted by both the ab initio PES and a Morse + Ling Rigby potential. Because the Morse + Ling–Rigby PES combination is not suitable for N–N_2 collisions, only N_2–N_2 collisions are considered, as described in [36]. Specifically, if N atoms are produced by a dissociating trajectory, they are simply removed from the simulation. Therefore, the rovibrational relaxation and dissociation results in Fig. 10 are interpreted as due to N_2–N_2 collisions only. We are interested in observing any differences in the QSS state predicted by the PESs. To study such differences, we initialize the N_2 system in thermal equilibrium (at 15,000, 20,000, and 30,000 K) and allow it to evolve into QSS.

Overall, the predictions of both PESs are very similar. Dissociation begins immediately and removes rotational and vibrational energy from the gas while the translational temperature is held constant to achieve isothermal relaxation. Ultimately, a QSS is reached where the excitation of rovibrational energy is balanced by removal due to dissociation. Rates of dissociation, captured by the decreasing amount of N_2, exhibit their largest discrepancy at the lowest temperature and appear nearly identical at the highest temperature. The average rotational and vibrational energies [defined by T_{rot} and T_{vib} in Eq. (7)] exhibit noticeable differences for all cases. In general, the rotational energies in QSS are in better agreement than the vibrational energies.

In Figs. 10a and 10c, it can be seen that, at time zero, $T_{\text{vib}} > T_{\text{rot}} > T_{\text{tra}}$. This results from the fact that initial molecular states correspond to quantized energy levels using the procedure described by Bender et al. [16]; however, the postprocessed temperature is obtained using the simple expression in Eq. (7). Alternate definitions for temperature, in terms of internal energy, are discussed in [29]. Finally, it is important to note that the QSS state is only a function of the isothermal translational temperature and is independent of the initial condition. This has been recently demonstrated by Grover et al. and can be seen in Fig. 1b of [39].

The vibrational EDFs in QSS predicted by both ab initio and Morse + Ling–Rigby PESs, seen in Fig. 10, appear almost identical; however, it is important to note that they are plotted on a log scale over many orders of magnitude. Upon close inspection, the differences in EDFs are consistent with the differences in average energy profiles (T_{rot} and T_{vib}). For example, in Fig. 10b, the vibrational energy population is higher for the ab initio PES, which is consistent with the higher value of T_{vib} in Fig. 10a compared to the corresponding Morse + Ling–Rigby results. In general, directly comparing results produced by different PESs may be useful in understanding what features of a PES are responsible for a macroscopic effect. Along these lines, DMS has recently been used to compare dissociation predictions for two ab initio PESs developed at the University of Minnesota and NASA Ames Research Center [39,40].

V. Conclusions

This paper summarized recent developments in the direct molecular simulation (DMS) method, originally developed by Koura [14,15] as the CTC–DSMC method. An implementation using the no-time-counter (NTC) collision rate algorithm, commonly used in DSMC, was described along with additional considerations required to incorporate DMS within a modern, parallel, DSMC code.

Similar to the molecular dynamics (MD) method, the sole model input to a DMS calculation is the potential energy surface (PES). DMS and pure MD results for shock waves were found to be identical, demonstrating that DMS acts as an acceleration technique for the MD simulation of dilute gases. Because the DMS method computes only the dominant energy transitions that occur during an evolving gas system, as opposed to precomputing all possible transition rates as required for master equation analysis, DMS is tractable for gas mixtures involving both atom–diatom and diatom–diatom collisions.

DMS predictions for rovibrational coupling were presented for normal shock-wave conditions relevant to hypersonic flight at 40 km altitude. DMS shock-wave simulations revealed direct rotational–vibrational energy coupling not modeled by the Jeans and Landau–Teller equations for translational–rotational and translational–vibrational relaxation, respectively. Direct rovibrational coupling was found to increase as the degree of anharmonicity of the potential energy surface (PES) increases and as the system temperature increases. However, such studies should be repeated by accounting for dissociation because dissociation may have a more dominant influence on the rovibrational state of the gas compared to the direct rovibrational coupling studied in this paper.

DMS results using an ab initio PES [16,32] were presented for a reacting nitrogen system involving both N_2–N_2 and N–N_2 collisions. The results highlight a number of physical phenomena described in greater detail in recent articles [16,34,36]. For translational temperatures at or below 10,000 K, rotational and vibrational energy excite at dramatically different rates, whereas at higher temperature, the excitation rates begin to approach each other. The vibrational energy distribution function exhibits non-Boltzmann behavior where high energy levels are overpopulated during initial excitation and depleted in the quasi-steady-state dissociating phase. As nitrogen atoms are produced, they efficiently excite the vibrational energy of nitrogen molecules through exchange reactions. Molecules with high vibrational and rotational energies are favored for dissociation reactions, although the favoring is stronger for vibrational energy.

Finally, the ability of DMS to rapidly compare macroscopic results from different PESs was demonstrated by simulating a dissociating nitrogen gas with both an ab initio PES and a simplified PES (Morse + Ling–Rigby). Surprisingly good agreement in the QSS region was found between the two simulation results; however, only N_2–N_2 collisions were considered in these particular simulations.

Overall, because of increases in both computational power and the accuracy of potential energy surfaces, DMS has become a useful numerical method to reveal new physics for nonequilibrium dilute gas flows. Using a PES (or library of PESs) as the model input, DMS calculations, although computationally expensive, can produce results at macroscopic scales that serve as high-fidelity, benchmark

data, which may aid the development and verification of nonequilibrium models. As presented in this paper, even two-dimensional DMS calculations are now possible.

Appendix A: Site-to-Site Potentials

Two site-to-site potentials are used in the current work to evaluate the forces between atoms that belong to different N_2 molecules. Such potentials characterize translational–rotational energy transfer.

The Lennard–Jones potential is given by

$$\phi(r) = 4\epsilon^{LJ}\left[\left(\frac{\sigma^{LJ}}{r}\right)^{12} - \left(\frac{\sigma^{LJ}}{r}\right)^{6}\right] \tag{A1}$$

where $\sigma^{LJ} = 3.17$ Å, and $\epsilon^{LJ}/k_B = 47.22$ K.

The Ling–Rigby potential is given by

$$\phi(r) = D_e \exp(-\alpha r - \beta r^2) - f_d(r)\frac{C_6}{r^6} \tag{A2}$$

where $D_e = 14151.94$ kcal/mol, $\alpha = 2.2412$ Å^{-1}, $\beta = 0.3214$ Å^{-2}, $C_6 = 33.6$ (kcal · Å^6)/mol, and $f_d(r)$ is the damping function:

$$f_d(r) = \exp\left(-\frac{1}{4}\left[\left(\frac{\delta}{r}\right)^2 - 1\right]\right) \tag{A3}$$

where $\delta = 4.14$ Å. For both potentials, r is the distance between atoms belonging to different N_2 molecules.

Appendix B: Intramolecular Potentials

Three intramolecular potentials are used in the current work to evaluate the forces on atoms that belong to the same N_2 molecule. Such potentials characterize vibrational energy and coupling with rotational energy.

The harmonic oscillator potential is given by

$$\phi(r) = \frac{1}{2}k_f(r - r_o)^2 \tag{B1}$$

The Taylor-6 potential is given by

$$\phi(r)/D_d = a^2(r - r_o)^2 - a^3(r - r_o)^3 + \frac{7}{12}a^4(r - r_o)^4 - \frac{1}{4}a^5(r - r_o)^5 + \frac{31}{360}a^6(r - r_o)^6 \tag{B2}$$

The Morse potential is given by

$$\phi(r) = D_d(1 - \exp\{-a[r - r_o]\})^2 \tag{B3}$$

In the preceding equations, the coefficient a is given by

$$a = \sqrt{\frac{k_f}{2D_d}} = 2.689\text{Å}^{-1} \tag{B4}$$

where $D_d = 227.6$ kcal/mol is the potential well depth, and k_f is the modeled spring constant. Finally, r is the distance between atoms belonging to the same N_2 molecule, and $r_o = 1.098$ Å is the equilibrium bond length.

Acknowledgments

The research is supported by the U.S. Air Force Office of Scientific Research (AFOSR) under grant FA9550-16-1-0161. The views and conclusions contained herein are those of the authors and should not be interpreted as necessarily representing the official policies or endorsements, either expressed or implied, of the AFOSR or the U.S. Government.

References

[1] Bird, G. A., *Molecular Gas Dynamics and the Direct Simulation of Gas Flows*, Oxford Univ. Press, New York, 1994, pp. 218–220.

[2] Boyd, I. D., and Schwartzentruber, T. E., *Nonequilibrium Gas Dynamics and Molecular Simulation*, Cambridge Univ. Press, New York, 2017, pp. 197–202.

[3] Kim, J. G., and Boyd, I. D., "State-Resolved Master Equation Analysis of Thermochemical Nonequilibrium of Nitrogen," *Chemical Physics*, Vol. 415, March 2013, pp. 237–246. doi:10.1016/j.chemphys.2013.01.027

[4] Panesi, M., Jaffe, R. L., Schwenke, D. W., and Magin, T. E., "Rovibrational Internal Energy Transfer and Dissociation of $N_2(^1\Sigma_g^+) - N(^4S_u)$ System in Hypersonic Flows," *Journal of Chemical Physics*, Vol. 138, No. 4, 2013, Paper 044312. doi:10.1063/1.4774412

[5] Jaffe, R. L., Schwenke, D. W., and Chaban, G., "Theoretical Analysis of N_2 Collisional Dissociation and Rotation–Vibration Energy Transfer," *47th AIAA Aerospace Sciences Meeting*, AIAA Paper 2009-1569, Jan. 2009.

[6] Zhu, T., Li, Z., and Levin, D. A., "Coarse-Grained Model for N_2–N Relaxation in Hypersonic Shock Conditions Using Two-Dimensional Bins," *AIP Conference Proceedings*, Vol. 1786, AIP Publishing, 2016, Paper 150008.

[7] Liu, Y., Panesi, M., Sahai, A., and Vinokur, M., "General Multi-Group Macroscopic Modeling for Thermo-Chemical Non-Equilibrium Gas Mixtures," *Journal of Chemical Physics*, Vol. 142, No. 13, 2015, Paper 134109.

[8] Andrienko, D., and Boyd, I. D., "Investigation of Oxygen Vibrational Relaxation by Quasi-Classical Trajectory Method," *Chemical Physics*, Vol. 459, Sept. 2015, pp. 1–13. doi:10.1016/j.chemphys.2015.07.023

[9] Andrienko, D. A., and Boyd, I. D., "High Fidelity Modeling of Thermal Relaxation and Dissociation of Oxygen," *Physics of Fluids*, Vol. 27, No. 11, 2015, Paper 116101.

[10] Andrienko, D. A., and Boyd, I. D., "Master Equation Study of Vibrational and Rotational Relaxations of Oxygen," *Journal of Thermophysics and Heat Transfer*, Vol. 30, No. 3, 2016, pp. 533–552.

[11] Andrienko, D. A., and Boyd, I. D., "Thermal Relaxation of Molecular Oxygen in Collisions with Nitrogen Atoms," *Journal of Chemical Physics*, Vol. 145, No. 1, 2016, Paper 014309. doi:10.1063/1.4955199

[12] Macdonald, R., Munafo, A., and Panesi, M., "Rovibrational Grouping for $N_2(^1\Sigma_g^+) - N_2(^1\Sigma_g^+)$ Energy Transfer Using State-to-State Model," *46th AIAA Thermophysics Conference*, AIAA Paper 2016-4315, 2016.

[13] Schwartzentruber, T. E., and Boyd, I. D., "Progress and Future Prospects for Particle-Based Simulation of Hypersonic Flow," *Progress in Aerospace Sciences*, Vol. 72, Jan. 2015, pp. 66–79. doi:10.1016/j.paerosci.2014.09.003

[14] Koura, K., "Monte Carlo Direct Simulation of Rotational Relaxation of Diatomic Molecules Using Classical Trajectory Calculations: Nitrogen Shock Wave," *Physics of Fluids*, Vol. 9, No. 11, 1997, pp. 3543–3549. doi:10.1063/1.869462

[15] Koura, K., "Monte Carlo Direct Simulation of Rotational Relaxation of Nitrogen Through High Total Temperature Shock Waves Using Classical Trajectory Calculations," *Physics of Fluids*, Vol. 10, No. 10, 1998, pp. 2689–2691. doi:10.1063/1.869782

[16] Bender, J. D., Valentini, P., Nompelis, I., Paukku, Y., Varga, Z., Truhlar, D. G., Schwartzentruber, T., and Candler, G. V., "An Improved Potential Energy Surface and Multi-Temperature Quasiclassical Trajectory Calculations of $N_2 + N_2$ Dissociation Reactions," *Journal of Chemical Physics*, Vol. 143, No. 5, 2015, Paper 054304. doi:10.1063/1.4927571

[17] Norman, P. E., "Atomistic Simulation of Non-Equilibrium Phenomena in Hypersonic Flows," Ph.D. Thesis, Univ. of Minnesota, Minnesota, MN, 2013.

[18] Gao, D., Zhang, C., and Schwartzentruber, T. E., "Particle Simulations of Planetary Probe Flows Employing Automated Mesh Refinement," *Journal of Spacecraft and Rockets*, Vol. 48, No. 3, 2011, pp. 397–405. doi:10.2514/1.52129

[19] Nompelis, I., and Schwartzentruber, T., "Strategies for Parallelization of the DSMC Method," *51st AIAA Aerospace Sciences Meeting*, AIAA Paper 2013-1204, 2013.

[20] Valentini, P., and Schwartzentruber, T. E., "A Combined Event-Driven/Time-Driven Molecular Dynamics Algorithm for the Simulation of Shock Waves in Rarefied Gases," *Journal of Computational Physics*, Vol. 228, No. 23, 2009, pp. 8766–8778. doi:10.1016/j.jcp.2009.08.026

[21] Valentini, P., and Schwartzentruber, T. E., "Large-Scale Molecular Dynamics Simulations of Normal Shock Waves in Dilute Argon," *Physics of Fluids*, Vol. 21, No. 6, 2009, Paper 066101.

[22] Valentini, P., Tump, P. A., Zhang, C., and Schwartzentruber, T. E., "Molecular Dynamics Simulations of Shock Waves in Mixtures of Noble Gases," *Journal of Thermophysics and Heat Transfer*, Vol. 27, No. 2, 2013, pp. 226–234. doi:10.2514/1.T3903

[23] Valentini, P., Zhang, C., and Schwartzentruber, T. E., "Molecular Dynamics Simulation of Rotational Relaxation in Nitrogen: Implications for Rotational Collision Number Models," *Physics of Fluids*, Vol. 24, No. 10, 2012, Paper 106101.

[24] Norman, P., Valentini, P., and Schwartzentruber, T. E., "GPU-Accelerated Classical Trajectory Calculation Direct Simulation Monte Carlo Applied to Shock Waves," *Journal of Computational Physics*, Vol. 247, Aug. 2013, pp. 153–167. doi:10.1016/j.jcp.2013.03.060

[25] Andersen, H. C., "Rattle: A 'Velocity' Version of the Shake Algorithm for Molecular Dynamics Calculations," *Journal of Computational Physics*, Vol. 52, No. 1, 1983, pp. 24–34. doi:10.1016/0021-9991(83)90014-1

[26] Zhang, C., Valentini, P., and Schwartzentruber, T. E., "Nonequilibrium-Direction-Dependent Rotational Energy Model for Use in Continuum and Stochastic Molecular Simulation," *AIAA Journal*, Vol. 52, No. 3, 2014, pp. 604–617. doi:10.2514/1.J052514

[27] Norman, P., and Schwartzentruber, T. E., "Classical Trajectory Calculation Direct Simulation Monte Carlo: Gpu Acceleration and Three Body Collisions," *51st AIAA Aerospace Sciences Meeting*, AIAA Paper 2013-1200, Jan. 2013.

[28] Bruno, D., Frezzotti, A., and Ghiroldi, G. P., "Oxygen Transport Properties Estimation by Classical Trajectory–Direct Simulation Monte Carlo," *Physics of Fluids*, Vol. 27, No. 5, 2015, Paper 057101.

[29] Valentini, P., Norman, P., Zhang, C., and Schwartzentruber, T. E., "Rovibrational Coupling in Molecular Nitrogen at High Temperature: An Atomic-Level Study," *Physics of Fluids*, Vol. 26, No. 5, 2014, Paper 056103.

[30] Morris, D. N., and Benson, P., "Data for ICBM Re-Entry Trajectories," Defense Technical Information Center, Rept. Accession #AD0405855, Fort Belvoir, VA, 1963.

[31] Morris, D. N., *Charts for Determining the Characteristics of Ballistic Trajectories in a Vacuum*, Rand Corp., Santa Monica, CA, 1964, pp. 23–43.

[32] Paukku, Y., Yang, K. R., Varga, Z., and Truhlar, D. G., "Global Ab Initio Ground-State Potential Energy Surface of N_4," *Journal of Chemical Physics*, Vol. 139, No. 4, 2013, Paper 044309. doi:10.1063/1.4811653

[33] Duchovic, R. J., Volobuev, Y. L., Lynch, G. C., Jasper, A. W., Truhlar, D. G., Allison, T. C., Wagner, A. F., Garrett, B. C., Espinosa-García, J., and Corchado, J. C., "POTLIB," http://comp.chem.umn.edu/potlib [retrieved 14 Jan. 2016].

[34] Valentini, P., Schwartzentruber, T. E., Bender, J. D., and Candler, G. V., "Direct Molecular Simulation of Nitrogen Dissociation Based on an Ab Initio Potential Energy Surface," *Physical Review Fluids*, Vol. 1, Aug. 2016, Paper 043402.

[35] Jaffe, R. L., "The Calculation of High-Temperature Equilibrium and Nonequilibrium Specific Heat Data for N_2, O_2 and NO," *22nd Thermophysics Conference*, AIAA Paper 1987-1633, 1987.

[36] Valentini, P., Schwartzentruber, T. E., Bender, J. D., Nompelis, I., and Candler, G. V., "Direct Molecular Simulation of Nitrogen Dissociation Based on an Ab Initio Potential Energy Surface," *Physics of Fluids*, Vol. 27, No. 8, 2015, Paper 086102.

[37] Kulakhmetov, M., Gallis, M., and Alexeenko, A., "Ab Initio-Informed Maximum Entropy Modeling of Rovibrational Relaxation and State-Specific Dissociation with Application to the $O_2 + O$ System," *Journal of Chemical Physics*, Vol. 144, No. 17, 2016, Paper 174302. doi:10.1063/1.4947590

[38] Singh, N., Valentini, P., and Schwartzentruber, T. E., "A Coupled Vibration-Dissociation Model for Nitrogen from Direct Molecular Simulation," *46th AIAA Thermophysics Conference*, AIAA Paper 2016-4318, 2016.

[39] Grover, M., Schwartzentruber, T. E., and Jaffe, R. L., "Dissociation and Internal Energy Excitation of Molecular Nitrogen due to $N + N_2$ Collisions Using Direct Molecular Simulation," *55th AIAA Aerospace Sciences Meeting*, AIAA Paper 2017-0660, 2017.

[40] Jaffe, R. L., Grover, M. S., Venturi, S., Schwenke, D., Valentini, P., Schwartzentruber, T. E., and Panesi, M., "Comparison of Quantum Mechanical and Empirical Potential Energy Surfaces and Computed Rate Coefficients for N_2 Dissociation," *Journal of Thermophysics and Heat Transfer*, Oct. 2017.